ACS APPLIED MATERIALS & INTERFACES

Research Article

www.acsami.org

Composition-Tuned ZnO/$Zn_xCd_{1-x}Te$ Core/Shell Nanowires Array with Broad Spectral Absorption from UV to NIR for Hydrogen Generation

Xueying Zhan,[†] Qisheng Wang,[†] Fengmei Wang,[†] Yajun Wang,[†] Zhenxing Wang,[†] Jinli Cao,[†,‡] Muhammad Safdar,[†] and Jun He*[,†]

[†]National Center for Nanoscience and Technology, Beijing 100190, P. R. China

[‡]School of Materials Science and Engineering, University of Science and Technology Beijing, Beijing 100083, P. R. China

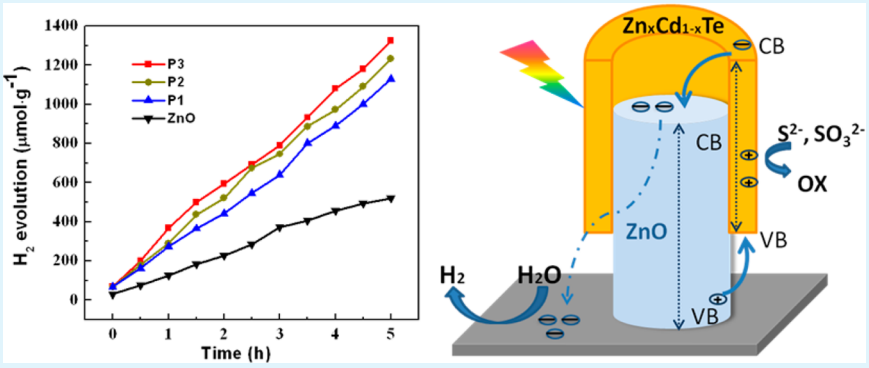

ABSTRACT: For highly efficient photoelectrodes, the materials used must have both a broad absorption range and large separation efficiency of photogenerated electron−hole pairs. Type II heterostructures with a ternary shell meet these two requirements and thus are recognized as being an ideal materials system for application in photocatalytic hydrogen production. Here, a ZnO/$Zn_xCd_{1-x}Te$ core/shell nanowires array with a broad absorption edge from UV (380 nm) to NIR (855 nm) was fabricated via a chemical vapor-deposition method. More importantly, the ZnO/$Zn_xCd_{1-x}Te$ core/shell nanowires array are highly single crystalline, and the composition can be continuously tuned by optimizing the deposition temperature, making the design of the desired photocatalyst possible. As expected, the single-crystalline ternary $Zn_xCd_{1-x}Te$ shell greatly enhances the charge separation efficiency and prolongs the lifetime of photogenerated charge carriers, which contribute to the high photocatalytic and photoelectrocatalytic activity under light irradiation. In addition, ZnO/$Zn_xCd_{1-x}Te$ core/shell structure show remarkable photocatalytic H_2-production activity and high H_2-production capability because of the synergistic light absorption of the ternary $Zn_xCd_{1-x}Te$ shell and the formation of a type II heterostructure at the interface between the ZnO core and $Zn_xCd_{1-x}Te$ shell. This work provides a new material platform for the design of highly efficient solar-fuel devices that demonstrate a broad and controllable absorption from the UV to NIR wavelengths.

KEYWORDS: *ZnO/$Zn_xCd_{1-x}Te$ nanowires array, controllable band gap, broad absorption, type II heterostructure, hydrogen production*

INTRODUCTION

The one-dimensional (1D) ZnO semiconductor has attracted considerable interest as the photoelectrode material for the conversion of water into the hydrogen because of its distinct merits of long photogenerated carrier lifetime, high electronic mobility, and facile synthesis.[1] However, its large band gap (3.37 eV) restricts its absorption in the ultraviolet region, which accounts for only 5% of the entire solar spectrum. As a result of the development of band-gap engineering, the absorption range of the 1D ZnO-based photoelectrode material has been extended to the visible light region by constructing type II core/shell heterostructure nanowires arrays with a narrower band-gap semiconductor such as CdS[2] or CdSe.[3] Importantly, the type II core/shell heterostructure nanowires array possesses four advantages: (1) the type II core/shell heterojunctions formed in the interfacial area of the core/shell heterostructures profoundly improve the separation efficiency of photogenerated electron−hole pairs,[4] (2) the large interfacial area of the core/shell heterostructure warrants fast charge separation and thus enhances the charge-collection efficiency,[5] (3) the shell of the heterostructure not only blocks nonradiative recombination of the electrons in ZnO cores with electrolyte but also provides protection of the ZnO cores from electrolyte-mediated corrosion,[6] and (4) the special topology of the 1D

Received: November 28, 2013
Accepted: January 27, 2014
Published: January 27, 2014

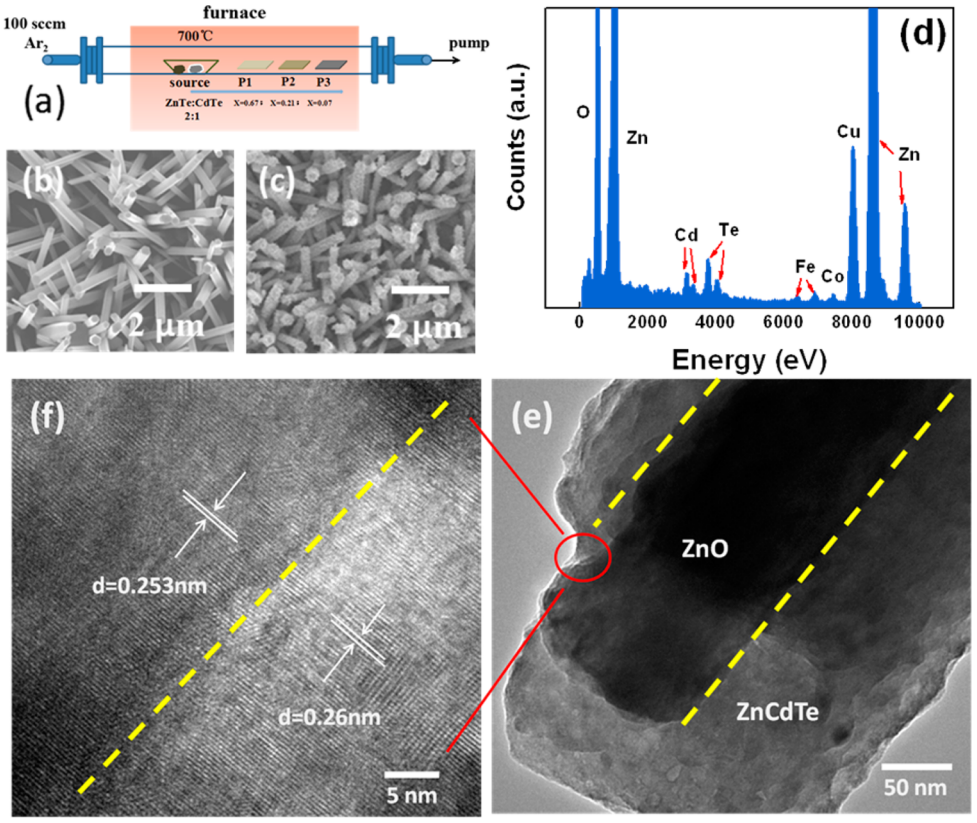

Figure 1. (a) Schematic diagram of the reactor setup. (b, c) SEM images of ZnO nanowires and ZnO/$Zn_xCd_{1-x}Te$ core/shell nanowires, repectively. (d) X-ray EDS of ZnO/$Zn_xCd_{1-x}Te$ core/shell nanowires. (e) TEM image of ZnO/$Zn_xCd_{1-x}Te$ core/shell nanowires. (f) Edge interface between the ZnO nanowire and $Zn_xCd_{1-x}Te$ shell.

nanostructure array offers a direct electric pathway for the rapid transport of photogenerated carriers to a conductive substrate.[7,8] As a result, much effort has been devoted to fabricating ZnO-based type II core/shell architecture nanowires arrays as photoelectrodes, including heterostructures with a binary shell, such as ZnO/CdS,[2] ZnO/CdTe,[9] ZnO/ZnSe,[10] and ZnO/In_2S_3,[11] and with a ternary shell, such as ZnO/ZnS_xSe_{1-x}[12] and ZnO/$Zn_xCd_{1-x}S$.[13]

In comparison to heterostructures with a binary shell, ZnO-based core/shell heterostructures with a ternary shell are more attractive because of their adjustable composition and band gap, which make the design of the desired photoelectrodes possible. Several synthesis techniques have been exploited to manufacture ternary shells. For example, an ion-exchange route has been applied to synthesize a $Zn_xCd_{1-x}Se$ ($0 < x < 1$) shell on a ZnO nanocables array, which demonstrated absorption covering almost the entire visible light region by modulating the shell composition.[14] Solvothermal methods have also been used to fabricate a $Zn_xCd_{1-x}S$ shell on a ZnO nanorods array, and their band gap can be controlled by regulating the Zn/Cd ratio during the synthesis process.[13] However, these methods involve complicated chemical reactions. In this way, the shell composition is strongly dependent on multiple chemical or physical factors such as chemical reagent concentration, solution temperature, and reaction time, which make it difficult to control the shell composition precisely. Thus, new strategies are required that can facilely and precisely adjust the chemical composition of a ternary shell.

The chemical-vapor deposition (CVD) technique provides an opportunity for the rational design of a ternary semiconductor shell with spatially graded compositions by simply controlling the deposition temperature.[15] For example, a composition-tunable $Zn_xCd_{1-x}Se$ ternary shell has been fabricated onto a pregrown ZnO nanowires array by temperature-gradient CVD.[16] Our group has also synthesized a ZnS_xSe_{1-x} ternary shell on a pregrown ZnO nanowires array by CVD.[12] However, the absorption edges of the ZnO/$Zn_xCd_{1-x}Se$ and ZnO/ZnS_xSe_{1-x} nanowires array only cover a narrow region of visible light because of the intrinsic large band gaps of these materials. Therefore, for highly efficient photoelectrodes, it is crucial to find a superior material to fabricate a ternary shell that has a much broader light absorption ability. The $Zn_xCd_{1-x}Te$ alloy shows a tunable band gap over a wide range from 2.25 to 1.45 eV and thus exhibits significant application potential for use in optoelectronics.[17,18] Consequently, ZnO/$Zn_xCd_{1-x}Te$ core/shell nanowires may show superior performance for water splitting. However, nothing has been reported on the growth of a composition-graded $Zn_xCd_{1-x}Te$ shell on a ZnO nanowires array or its application in photocatalytic hydrogen product.

In this work, a ternary alloy semiconductor with a $Zn_xCd_{1-x}Te$ shell was constructed by a simple CVD method on a ZnO nanowires array. By optimizing the experimental conditions, the Zn content of the $Zn_xCd_{1-x}Te$ shell can be gradually adjusted from 0 to 1 by simply controlling the deposition location in the CVD furnace. The absorption edge of this ZnO/$Zn_xCd_{1-x}Te$ core/shell nanostructure can be extended from the UV (380 nm) to the NIR (855 nm) region with an increase of the Cd composition, which covers nearly 22% of the entire solar spectrum. In addition, the synthesized

dx.doi.org/10.1021/am4054332 | ACS Appl. Mater. Interfaces 2014, 6, 2878−2883

$Zn_xCd_{1-x}Te$ shell is highly crystalline, which favors the fast transport of photogenerated carriers. Electrochemical impedance spectroscopy (EIS) was employed to investigate the charge-transfer and recombination processes. The results demonstrate that the $Zn_xCd_{1-x}Te$ shell-decorated ZnO nanowires array has an enhanced photoelectrochemical (PEC) performance. Significantly, the $Zn_xCd_{1-x}Te$ shell profoundly enhances the yield of hydrogen from the ZnO nanowires array. The ZnO/$Zn_xCd_{1-x}Te$ nanowires array developed in our work provides a new platform for the design of highly efficient solar cells and photocatalysts.

EXPERIMENTAL SECTION

ZnO/$Zn_xCd_{1-x}Te$ Core/Shell Nanowires Array Synthesis. The ZnO/$Zn_xCd_{1-x}Te$ core/shell nanowires array was prepared on ITO substrates by a two-step process: growth of the ZnO nanowires array by a hydrothermal method[19] and deposition of the $Zn_xCd_{1-x}Te$ shell on the pregrown ZnO nanowires array by CVD. In the first step, the ITO substrates were chemically cleaned by ethanol and then exposed to UV irradiation. After that, the ITO substrates were seeded by a ZnO nanoballs layer. Then, the substrates were placed in an aqueous solution of 25 mM zinc nitrate hexahydrate ($Zn(NO_3)_2{\cdot}6H_2O$) and 25 mM hexamethylenetetramine (HMT), which was heated at 90 °C. After 8 h, the samples were washed by deionized water and dried in air at 60 °C. In the second step, $Zn_xCd_{1-x}Te$ shells were coated onto a pregrown ZnO nanowires array by CVD. After the growth of ZnO nanowires on the ITO substrate, three pregrown samples (P1−P3) were placed downstream of the gas flow. A mixture of high-purity ZnTe and CdTe powders (Alfa Aesar, 99.99%) with a ratio of 2:1 was placed in the center of the furnace as the vapor source. The distance between the ITO substrate and source ranged from 8 to 12 cm. A schematic diagram of the reactor setup is shown in Figure 1a. The furnace was heated at 700 °C by two steps as follows: first from room temperature to 500 °C at a rate of 70 °C/min and then from 500 to 700 °C with a rate of 100 °C/min. Once sample heating was completed, the furnace was cooled to room temperature rapidly under an argon gas atmosphere at a flow rate of 100 sccm.

XRD and Absorption Measurements. Elemental composition analysis was determined by X-ray diffraction (XRD) on an (Philips X'Pert Pro Super) X-ray powder diffractometer with Cu Kα radiation (λ = 1.5418 Å). UV−vis−NIR diffuse reflectance spectroscopy (DRS) of the ZnO/$Zn_xCd_{1-x}Te$ core/shell nanowires array was performed with a Hitachi U-3100 in diffuse reflection mode with a range of 300−900 nm.

Photoelectrochemical Measurements. Photoelectrochemical properties of the ZnO/$Zn_xCd_{1-x}Te$ core/shell nanowires array were determined on a CHI650D electrochemical system (Shanghai, China). All photoelectrochemical measurements were taken in a rectangular quartz reactor electrolyte solution with a standard three-electrode system: ZnO/$Zn_xCd_{1-x}Te$ core/shell nanowires array, working electrode; Pt wire, counter electrode; and standard calomel electrode (SCE), reference electrode. The as-prepared electrode was immersed into a 0.1 M Na_2SO_4 electrolyte solution with an area of 2 × 3 cm^2. The photoresponses were measured under a 500 W xenon lamp (Beijing China Education Au-light Co. Ltd.) with a 420 nm cutoff filter at 0.0 V versus SCE. Here, the incident light intensity is maintained at 377 mW/cm^2.

Photocatalytic H_2 Evolution Measurements. The photocatalytic H_2 evolution by water-splitting experiments was conducted in a 300 mL pyrex reactor under photoirradiation conditions that was coupled with a gas chromatograph (TianmeiGC-7900) equipped with a thermal conductivity detector. A 300 W xenon lamp with a cutoff filter (250 < λ < 780 nm, 751.6 mW/cm^2) was used to irradiate the suspension. In a typical H_2-production experiment, two pieces of pure ZnO, P1−P3 samples, respectively, were placed at the bottom of a quartz reactor containing 80 mL of a mixed aqueous solution with 0.25 M Na_2SO_3 and 0.35 M Na_2S as sacrificial agents. Before irradiation, the system was bubbled with Argon for 1 h to remove the air and to ensure that the system was under anaerobic conditions. A certain amount of gas was sampled through the septum. Meanwhile, the generated H_2 was analyzed by gas chromatography.

RESULTS AND DISCUSSION

The morphology and microstructure of the as-prepared ZnO/$Zn_xCd_{1-x}Te$ core/shell nanowires array were examined by Hitachi S-4800 field-emission scanning electron microscopy (FE-SEM) and FEI Tecnai F20 high-resolution transmission electron microscopy (HRTEM). A typical SEM image of ZnO nanowires grown on ITO substrates is shown in Figure 1b. The diameters of pristine ZnO nanowires ranged from 50 to 150 nm. After coating with $Zn_xCd_{1-x}Te$, the diameters of the ZnO/$Zn_xCd_{1-x}Te$ core/shell nanowires array increased to 100−200 nm, as displayed in Figure 1c, and the surface of the pristine ZnO nanowires became rough. Figure 1d shows an X-ray energy-dispersive spectrum (EDS) acquired from sample P2. The peak intensities of Cd and Te gives their atomic ratio as 0.89 to 1.58. The elements Cd and Te likely come from the ternary $Zn_xCd_{1-x}Te$ shell. To obtain further information on the microstructure and crystallinity of the ZnO/$Zn_xCd_{1-x}Te$ core/shell nanowires array, TEM and HRTEM were carried out on sample P2. In Figure 1e, it can be clearly seen that the ZnO nanowire is covered by a 50 nm thick $Zn_xCd_{1-x}Te$ shell with a distinct interface between the ZnO nanowire and $Zn_xCd_{1-x}Te$ shell. Note that the $Zn_xCd_{1-x}Te$ shell is highly crystalline with an interplanar spacing of 0.253 nm, as exhibited in Figure 1f. The highly crystalline nature of the $Zn_xCd_{1-x}Te$ shell is beneficial for the separation and transfer of photogenerated carriers. The measured interplanar spacing of the ZnO core is 0.26 nm, which is consistent with that of the (001) plane of ZnO.

To analyze the elemental composition of the different samples, XRD of all samples was performed, as shown in Figure 2a. For comparison, the XRD patterns of a pristine ZnO nanowires array grown on ITO substrate, pure CdTe powder, and pure ZnTe powder are also shown. Samples P1−P3 all show weak peaks at 23.6° (marked by black squares), corresponding to the (111) plane of cubic CdTe (JCPDS 65-1082). They also display peaks at 65.8° (black stars) which is consistent with (331) plane of cubic ZnTe (JCPDS 65-385). The presence of these two peaks on all samples proves that the shell is composed of ternary $Zn_xCd_{1-x}Te$. In addition, all samples show a peak at around 29.1°, which belongs to the (111) plane of cubic ZnTe. This peak gradually increases from 28.5° in P1 to 27.5° in P2 and 27.4° in P3 (labeled by black triangles). The trend is in accordance with Vegard's law.[20] It is known that the ionic radius of Cd^{2+} ions (95 pm) is slightly longer than that of Zn^{2+} ions (74 pm).[21] As more Zn^{2+} ions are substituted by Cd^{2+} ions in samples P1−P3, the interplanar spacing of the (111) plane gradually increases. As a result, the diffraction angle continuously decreases. In addition, all samples exhibit peaks at 31.8, 34.5, 36.2, and 56.6°, which are indexed to the (100), (002), (101), and (110) planes of hexagonal ZnO (JCPDS 89-510), respectively. Obviously, these strong XRD peaks are caused by the ZnO nanowires core. The XRD peak of the ITO substrate at 30.4° also appears for all samples as well as the pristine ZnO nanowires array grown on the ITO substrate.

To confirm the Zn content of different $Zn_xCd_{1-x}Te$ shells further, UV−vis−NIR DRS of the ZnO/$Zn_xCd_{1-x}Te$ core/shell nanowires was studied, as shown in Figure 2b. The pristine ZnO nanowires array on ITO substrates shows an absorption peak located at ∼380 nm, corresponding to the expected band

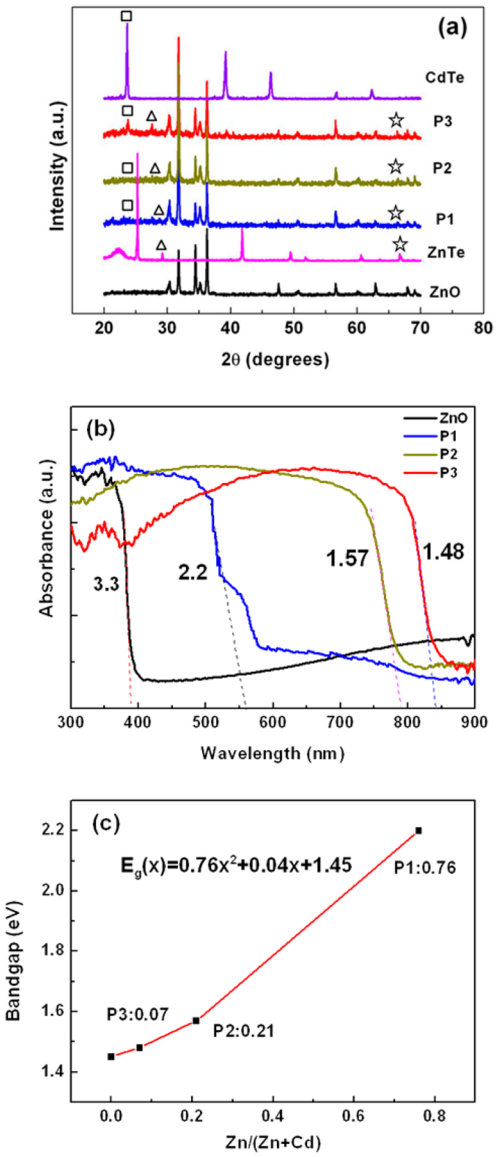

Figure 2. (a) XRD data of ZnO/$Zn_xCd_{1-x}Te$ core/shell nanowires on ITO substrates with different Zn concentrations (samples P1−P3). For comparison, XRD data of pristine ZnO nanowires, pure CdTe powder, and pure ZnTe powder are also given. (b) UV−vis DRS spectra of pristine ZnO nanowire arrays and ZnO/ZnS_xSe_{1-x} core/shell nanowire arrays (samples P1−P3). (c) Plot of the band gap of the ZnO/ZnS_xSe_{1-x} core/shell vs Zn concentration.

gap (3.3 eV). After coating with $Zn_xCd_{1-x}Te$ shells, the absorption of the ZnO/$Zn_xCd_{1-x}Te$ core/shell nanowires is extended to the entire visible light region and part of the NIR region. Importantly, the absorption edges of the samples decrease step-by-step from 2.20 eV for P1 to 1.57 eV for P2 and 1.48 eV for P3 with the increasing Cd content, indicating that the band gap of the ternary semiconductor compound can be adjusted through tuning the element composition. For the $Zn_xCd_{1-x}Te$ shells, nonlinear band gaps are dependent on the composition of Zn or Cd. Here, Zn content, x, can be fitted through a quadratic relationship as follows

$$E_g(x) = xE_g(\mathrm{ZnTe}) + (1-x)E_g(\mathrm{CdTe}) - x(1-x)b \quad (1)$$

where $E_g(x)$, E_g(ZnTe), and E_g(CdTe) are the band gaps of $Zn_xCd_{1-x}Te$, ZnTe, and CdTe, respectively. According to the literature,[17,18] the band gaps of ZnTe and CdTe are 2.25 and 1.45 eV, respectively, and b, the bowing parameter, is set as 0.76.[22] Therefore, the Zn concentration, x, of samples P1−P3 is calculated to be 0.76, 0.21 and 0.07, respectively. Figure 2c shows the plots of Zn composition versus band gap of the $Zn_xCd_{1-x}Te$ shell. The band gap of the $Zn_xCd_{1-x}Te$ shell continuously increases with an increase of the Zn composition. Consequently, the band gap of the ZnO/$Zn_xCd_{1-x}Te$ core/shell nanowires can be modulated by controlling the deposition location of the samples.

Electrochemical measurements were performed to investigate the PEC properties of ZnO/$Zn_xCd_{1-x}Te$ electrodes under visible-light irradiation (λ > 420 nm). Figure 3a shows the amperometric current−time ($I-t$) curves of different samples (P1−P3) at 0 V versus SCE with the light on and off. When the light turns on, the photocurrent density of sample P1 sharply increases from 0.1 to 0.76 μA/cm^2. As for P2, the dark current density is 0.05 μA/cm^2, and the photocurrent density is 2.25 μA/cm^2. Sample P3 has the same dark current density as P2 but a higher photocurrent density, 5.45 μA/cm^2. However, the pregrown ZnO nanowires array photoelectrode has no distinct photoresponse under visible-light irradiation because of its large band gap (3.3 eV). These results suggest that (1) compared with pristine ZnO nanowires photoelectrodes, the photoelectrodes coated by $Zn_xCd_{1-x}Te$ shells significantly improve visible-light absorption efficiency and (2) with the increase in Cd content from P1−P3, the visible-light absorption range gradually increases, which is consistent with the results of UV−vis−NIR DRS. Electrochemical impedance spectroscopy (EIS) is considered to be a powerful tool to study charge-transfer and recombination processes of photoelectrodes. EIS Nyquist plots of ZnO and ZnO/$Zn_xCd_{1-x}Te$ photocatalysts under visible-light irradiation are presented in Figure 3b. The arc radius of the ZnO/$Zn_xCd_{1-x}Te$ electrodes (P1−P3) is much smaller than that of the pristine ZnO electrode under visible-light irradiation, which suggests that introduction of a $Zn_xCd_{1-x}Te$ shell on the ZnO nanowires array notably improves separation efficiency of photogenerated electron−hole pairs and thus reduces charge-transfer resistances.[23,24] In addition, with the increase in Cd content from P1−P3, the arc radius gradually decreases. This is likely because the visible-light absorption range of P3 is much larger than those of P2 and P1. As a result, more photogenerated carriers are produced inside sample P3, leading to smaller impedance.

Figure 4 shows the photocatalytic H_2-production activity of samples P1−P3 from an aqueous solution containing Na_2S and Na_2SO_3 under UV−vis irradiation together with that of pristine ZnO nanowires for comparison. As shown in Figure 4a, the photocatalytic H_2-production activity of pure ZnO nanowires is revealed during 5 h of light illumination. With the presence of $Zn_xCd_{1-x}Te$, the H_2-evolution property is remarkably enhanced. The amount of H_2 generated on the basis of sample P3 reaches 1.326 mmol/g, which is over 2-fold greater than that of pure ZnO nanowires (0.522 mmol/g). Note that the amount of H_2 generated increases with the increase in the Cd content,[25] which is consistent with the PEC results. Moreover, the rate of H_2 evolution of the samples in Figure 4b shows a value of 265 μmol h^{-1} g^{-1} for sample P3. The pristine ZnO nanowires on ITO substrate, however, give an evolution rate of 104 μmol h^{-1} g^{-1}. These results demonstrate that the presence of the $Zn_xCd_{1-x}Te$ crystalline shell is crucial for the improved

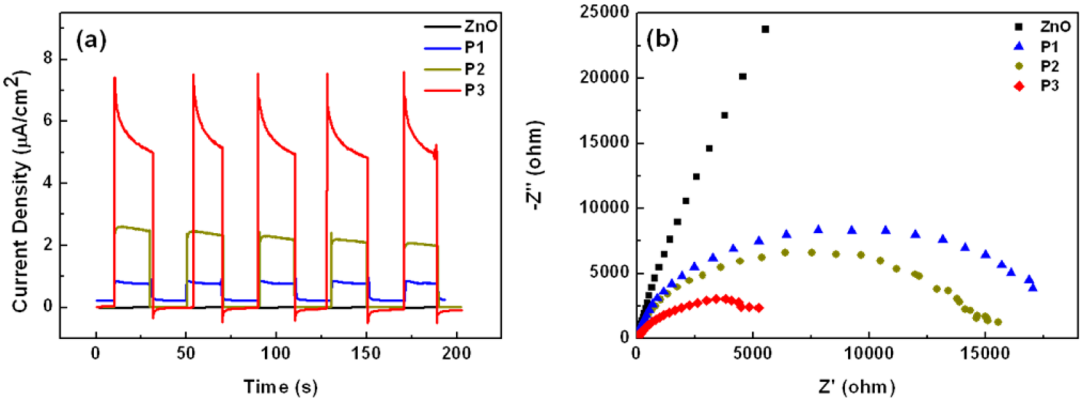

Figure 3. (a) Photoelectrochemical responses and (b) Nyquist plots of EIS of ZnO and ZnO/$Zn_xCd_{1-x}Te$ core/shell nanowires array electrodes (P1− P2, and P3) under visible-light irradiation (λ > 420 nm) ([Na_2SO_4] = 0.1 M).

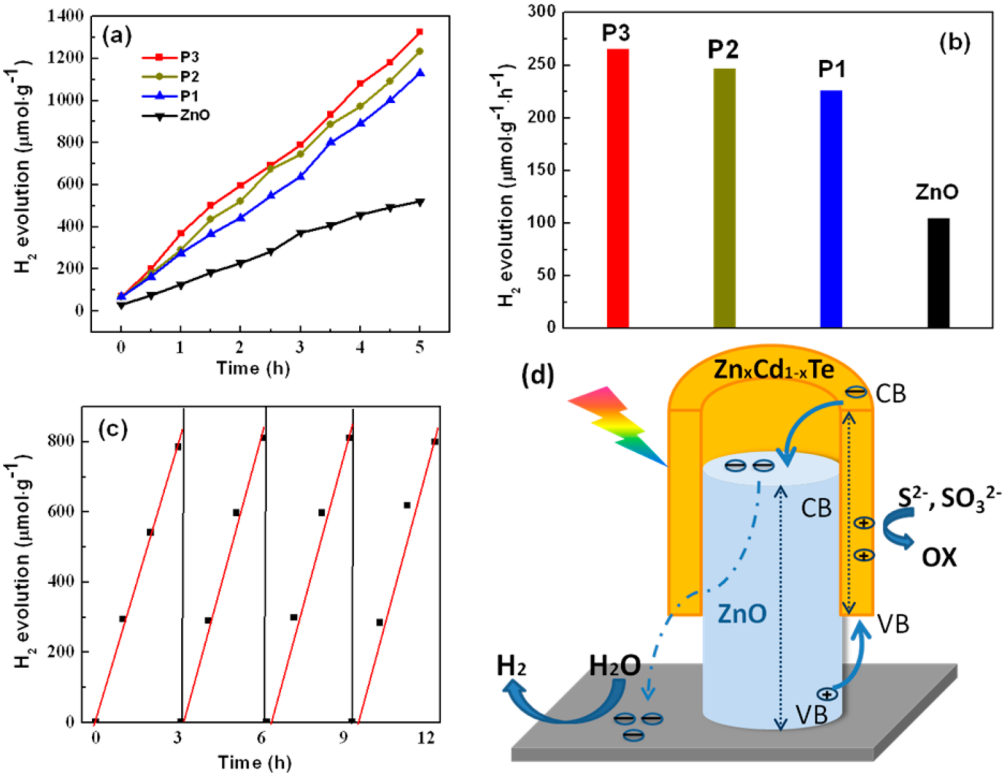

Figure 4. (a) Photocatalytic H_2-production activity of the pristine ZnO nanowires, samples P1−P3, from an aqueous solution containing Na_2S and Na_2SO_3 under UV−vis irradiation. (b) Rate of H_2 evolution of the pristine ZnO nanowires, samples P1−P3. (c) H_2-production capability of sample P3 from an aqueous solution containing Na_2S and Na_2SO_3 under the sameUV−vis irradiation over 12 h. (d) Schematic illustration for charge transfer and separation in the ZnO/$Zn_xCd_{1-x}Te$ core/shell nanowires array.

performance of these photocatalysts. As a result, the H_2-production efficiency increase by ∼2.6-fold when exposed to UV−vis irradiation when Na_2S/Na_2SO_3 are used as hole scavengers. Furthermore, with variation of x in $Zn_xCd_{1-x}Te$ from 0.76 to 0.07, the photocatalytic activity increases from 226 to 265 μmol h^{-1} g^{-1} because of the enhancement of visible-light absorption efficiency. Throughout the testing cycles displayed in Figure 4c, sample P3 exhibites a persistent high H_2-production capability. Therefore, the crystalline $Zn_xCd_{1-x}Te$ shell protects the ZnO nanowires to some extent during the light irradiation. The mechanism of the H_2-production performance of ZnO/$Zn_xCd_{1-x}Te$ electrodes (P1−P3) can be elucidated by the schematic illumination of electron−hole separation and transport at the ZnO/$Zn_xCd_{1-x}Te$ interface in Figure 4d. As known, the light-absorption capability of a semiconductor is a crucial factor for photocatalytic H_2 production.[26,27] The ZnO/$Zn_xCd_{1-x}Te$ core/shell structure remarkably extends the absorption range of light from UV to NIR, which greatly enhances the light-absorption capability in comparison with pure ZnO nanowires. However, it is worth noting that photogenerated carriers will reconbine fast, leading to a low photocatalytic H_2 production.[28] In this work, a single crystalline $Zn_xCd_{1-x}Te$ shell and well-aligned ZnO/$Zn_xCd_{1-x}Te$ interface were achieved by optimizing the CVD conditions. Thus, the built-in field formed at the type II heterostructure interface favors the vertical transfer of photogenerated electrons from the CB of $Zn_xCd_{1-x}Te$ to the CB of ZnO, which provides a direct path for electron transfer. The H^+

dx.doi.org/10.1021/am4054332 | ACS Appl. Mater. Interfaces 2014, 6, 2878−2883

in the solution is then reduced to a hydrogen molecule with the photogenerated electrons collected on ITO substrates. Meanwhile, the holes are transferred to the valence band (VB) of the $Zn_xCd_{1-x}Te$ shell and then consumed by the sacrificial agents (S^{2-} and SO_3^{2-}). Consequently, the photogenerated charge-separation efficiency is improved because of the declining charge-recombination rate.[4,29] Moreover, the increase of the spectra absorption range mentioned above is also crucial to obtain better H_2-production performance of the ZnO/$Zn_xCd_{1-x}Te$ core/shell nanostructure than that of pristine ZnO nanowires.[30] For the ZnO/$Zn_xCd_{1-x}Te$ core/shell nanostructure, a significant advantage should be noted: the ternary shell $Zn_xCd_{1-x}Te$ band could be tuned over a large range from ZnTe (2.25 eV, ~550 nm) to CdTe (1.45 eV, ~855 nm) as the x value increases from 1 to 0, which enhances the visible-light absorption of the whole system. Although the position of the band changes as the x value decreases, we have to notice that the band alignment between the core and shell always keeps the type II structure.

CONCLUSIONS

We have synthesized a composition-graded ZnO/$Zn_xCd_{1-x}Te$ core/shell nanowires array on ITO substrates via a hydrothermal method followed by a CVD method. Through controlling the deposition location, the Zn content of the shells can be continuously and exactly tuned from 0 to 1. TEM results explicitly reveal that the $Zn_xCd_{1-x}Te$ shell is highly crystalline and covers the entire surface of the ZnO nanowire. Importantly, the ZnO/$Zn_xCd_{1-x}Te$ core/shell nanowires array shows a broad absorption range from UV to NIR by adjusting the shell composition. The introduction of the $Zn_xCd_{1-x}Te$ shell to the ZnO nanowires also profoundly improves the photogenerated charge-separation process because of the formation of a type II heterojunction at the interface. As expected, an enhanced yield of hydrogen was observed after coating the ZnO nanowires with a $Zn_xCd_{1-x}Te$ shell. These results are of great significance for the design of composition-modulated core/shell electrodes with a large and controllable absorption range from UV to NIR.

AUTHOR INFORMATION

Corresponding Author

*E-mail: hej@nanoctr.cn.

Notes

The authors declare no competing financial interest.

ACKNOWLEDGMENTS

This work was supported by the 973 Program of the Ministry of Science and Technology of China (no. 2012CB934103), the 100-Talents Program of the Chinese Academy of Sciences (no.Y1172911ZX), and the National Natural Science Foundation of China (nos. 21373065 and 21307020).

REFERENCES

(1) Huang, J.; Yin, Z.; Zheng, Q. *Energy Environ. Sci.* **2011**, *4*, 3861−3877.
(2) Tak, Y.; Hong, S. J.; Lee, J. S.; Yong, K. *J. Mater. Chem.* **2009**, *19*, 5945−5951.
(3) Wang, G.; Yang, X.; Qian, F.; Zhang, J. Z.; Li, Y. *Nano Lett.* **2010**, *10*, 1088−1092.
(4) Wang, Y.; Wang, Q.; Zhan, X.; Wang, F.; Safdar, M.; He, J. *Nanoscale* **2013**, *5*, 8326−8339.
(5) Tsakalakos, L. *Mater. Sci. Eng., R* **2008**, *62*, 175−189.
(6) Seol, M.; Kim, H.; Tak, Y.; Yong, K. *Chem. Commun.* **2010**, *46*, 5521−5523.
(7) Lauhon, L. J.; Gudiksen, M. S.; Wang, D.; Lieber, L. B. *Nature* **2002**, *420*, 57−61.
(8) Zhang, Y.; Wang, L.; Mascarenhas, A. *Nano Lett.* **2007**, *7*, 1264−1269.
(9) Wang, X.; Zhu, H.; Xu, Y.; Wang, H.; Tao, Y.; Hark, S.; Xiao, X.; Li, Q. *ACS Nano* **2010**, *4*, 3302−3308.
(10) Wu, Z.; Zhang, Y.; Zheng, J.; Lin, X.; Chen, X.; Huang, B.; Wang, H.; Huang, K.; Li, S.; Kang, J. *J. Mater. Chem.* **2011**, *21*, 6020−6026.
(11) Strothkämper, C.; Schwarzburg, K.; Schütz, R.; Eichberger, R.; Bartelt, A. *J. Phys. Chem. C* **2012**, *116*, 1165−1173.
(12) Wang, Z.; Zhan, X.; Wang, Y.; Safdar, M.; Niu, M.; Zhang, J.; Huang, Y.; He, J. *Appl. Phys. Lett.* **2012**, *101*, 073105−073110.
(13) Xie, S.; Lu, X.; Zhai, T.; Gan, J.; Li, W.; Xu, M.; Yu, M.; Zhang, Y. M.; Tong, Y. *Langmuir* **2012**, *28*, 10558−10564.
(14) Xu, J.; Yang, X.; Wang, H.; Chen, X.; Luan, C.; Xu, Z.; Lu, Z.; Roy, V. A.; Zhang, W.; Lee, C. S. *Nano Lett.* **2011**, *11*, 4138−4143.
(15) Zhuang, X.; Ning, C. Z.; Pan, A. *Adv. Mater.* **2012**, *24*, 13−33.
(16) Li, H.; Cheng, C.; Li, X.; Liu, J.; Guan, C.; Tay, Y. Y.; Fan, H. J. *J. Phys. Chem. C* **2012**, *116*, 3802−3807.
(17) Durose, K.; Edwards, P. R.; Halliday, D. P. *J. Cryst. Growth* **1999**, *197*, 733−742.
(18) Zanio, K.; Willardson, R. K.; Beer, A. C. *Semicond. Semimetals* **1978**, *13*, 125−129.
(19) Lupan, O.; Guérin, V. M.; Tiginyanu, I. M.; Ursaki, V. V.; Chow, L.; Heinrich, H.; Pauporté, T. *J. Photochem. Photobiol., A* **2010**, *211*, 65−73.
(20) Vegard, L. Z. *Z. Phys.* **1921**, *5*, 17−26.
(21) Xing, C.; Zhang, Y.; Yan, W.; Guo, L. *Int. J. Hydrogen Energy* **2006**, *31*, 2018−2024.
(22) Becerril, M.; Silva-Lópe z, H.; Zelaya-Angel, O. *Rev. Mex. Fis.* **2004**, *50*, 588−593.
(23) Wang, Y.; Shi, R.; Lin, J.; Zhu, Y. *Energy Environ. Sci.* **2011**, *4*, 2922−2929.
(24) Wang, Y.; Bai, X.; Pan, C.; He, J.; Zhu, Y. *J. Mater. Chem.* **2012**, *22*, 11568−11573.
(25) Lingampalli, S. R.; Gautam, U. K.; Rao, C. N. R. *Energy Environ. Sci.* **2013**, *6*, 3589−3594.
(26) Liu, G. J.; Zhao, L.; Ma, L. J.; Guo, L. *Catal. Commun.* **2008**, *9*, 126−130.
(27) Xing, C. J.; Zhang, Y. J.; Yan, W.; Guo, L. J. *Int. J. Hydrogen Energy* **2006**, *31*, 2018−2024.
(28) Zhang, J.; Yu, J. G.; Jaroniec, M.; Gong, J. R. *Nano Lett.* **2012**, *12*, 4584−4589.
(29) Wang, Z.; Yin, H.; Jiang, C.; Safdar, M.; He, J. *Appl. Phys. Lett.* **2012**, *101*, 253109−253114.
(30) Miao, J. W.; Yang, H. B.; Khoo, S. Y.; Liu, B. *Nanoscale* **2013**, *5*, 11118−11124.